Article citation info:
CUI J, REN Y, XU B, YANG D, ZENG S. Reliability analysis of a multi-ESO based control strategy for level adjustment control system of quadruped robot under disturbances and failures. Eksploatacja i Niezawodnosc – Maintenance and Reliability 2020; 22 (1): 42–51, http://dx.doi.org/10.17531/ein.2020.1.6.

Jingjing CUI
Yi REN
Binghui XU
Dezhen YANG
Shengkui ZENG

RELIABILITY ANALYSIS OF A MULTI-ESO BASED CONTROL STRATEGY FOR LEVEL ADJUSTMENT CONTROL SYSTEM OF QUADRUPED ROBOT UNDER DISTURBANCES AND FAILURES

ANALIZA NIEZAWODNOŚCI STRATEGII STEROWANIA W OPARCIU O KILKA OBSERWATORÓW STANU ROZSZERZONEGO ESO I JEJ ZASTOSOWANIE W SYSTEMIE KONTROLI REGULACJI POZIOMU CZWORONOŻNEGO ROBOTA W WARUNKACH ZAKŁÓCEŃ I USZKODZEŃ

The complexity of control algorithms and their vulnerability to disturbances and failures are the main problems that restrict the operations of multi-legged mobile robots in more complex environments. In this paper, a multiple extended state observer (ESO) based control strategy is proposed to achieve stable tilt angle control for quadruped robots under the influence of disturbances and actuator failures. By treating the multiple legs as parallel control objects, more ESOs were added to improve the disturbance rejection ability of the linear active disturbance rejection control (LADRC). Correlation of interactive information about the legs is realized by the synthesis of multiple ESO information. Based on LADRC, this method has the advantages of easy parameter tuning, good robustness, and strong ability to cope with interference and fault conditions. A control system reliability evaluation method was proposed. The reliability and control performance of the multi-ESO based control system under leg stuck failure conditions were systematically analyzed. Simulation and experimental results for the level adjustment control system of a quadruped robot are provided to verify the disturbance rejection ability, feasibility and practicability of the proposed multi-ESO based control method.

Keywords: *reliability analysis, fault tolerance, active disturbance rejection control (ADRC), quadruped robots.*

Złożoność algorytmów sterowania oraz ich brak odporności na zakłócenia i uszkodzenia to główne czynniki ograniczające pracę wielonożnych robotów mobilnych w bardziej złożonych środowiskach. W przedstawionym artykule zaproponowano strategię sterowania wykorzystującą kilka obserwatorów stanu rozszerzonego (ESO), która pozwala na uzyskanie stabilnego kąta pochylenia robota czworonożnego w warunkach zakłóceń i uszkodzeń siłowników. Traktując każdą z nóg jako równorzędny obiekt sterowania, dodano dodatkowe ESO, co pozwoliło na poprawienie zdolności algorytmu liniowego aktywnego tłumienia zakłóceń (LADRC) do kompensacji (tłumienia) tych ostatnich. Interaktywne informacje dotyczące poszczególnych nóg korelowano poprzez syntezę danych z ESO. Zaletami omawianej metody opartej na LADRC są: łatwość dostrajania parametrów, wysoka niezawodność oraz bardzo dobra zdolność do radzenia sobie z zakłóceniami i uszkodzeniami. Zaproponowano także metodę oceny niezawodności systemu sterowania. Analizowano niezawodność i wydajność systemu opartego na kilku ESO w warunkach awarii wywołanej zablokowaniem nóg robota. Przedstawiono wyniki badań symulacyjnych i eksperymentalnych systemu sterowania regulacją poziomu robota czworonożnego, które pozwalają zweryfikować zdolność proponowanej metody do tłumienia zakłóceń, a także możliwość jej praktycznego zastosowania.

Słowa kluczowe: *analiza niezawodności, tolerancja uszkodzeń, aktywne tłumienie uszkodzeń (ADRC), roboty czworonożne.*

1. Introduction

With the rapid development of technology and increase in performance requirements, the complexity of multi-legged robots has increased in terms of mechanical structures and control algorithms, which has led to challenges in guaranteeing the reliability of the systems. To achieve reliability requirements, stable control under the influence of disturbances and failures is critical for multi-legged mobile robot systems. Researchers have made efforts to promote the reliability and disturbance rejection ability of mobile robot control systems. Intelligent distributed control [3,17,22,34] and fault-tolerant control [8,23-25] are the main solutions. Christensen et al. [2] designed a distributed control strategy for self-reconfigurable modular robots. Cully et al. [5] proposed an intelligent self-adaption control method for a six-legged robot. The researchers attempted to use intelligent distribution methods to address interactions and information crossover between multiple actuators. In the literature [4], a series control scheme based on active disturbance rejection control (ADRC)

is presented for mobile robots to improve their reliability under actuator failure without changing parameters, but only a 2-dimensional tilt angle of the mobile robot is considered. Through mathematical formula derivations, Kommuri [12] designed an observer-based sensor fault-tolerant control for electric vehicles. Xiao and Yin [27] designed a sliding mode observer to enhance fault-tolerant control of nonlinear systems with disturbance and actuator faults. Observer-based control methods can effectively capture the disturbances and faults caused by an uncertain environment, and then, the corresponding fault-tolerant control algorithms can be designed.

Although these methods have a certain effect on improving system reliability, the design process needs to obtain enough information, including object functions, mechanical dynamics, possible failure modes, effects, reasons and modeling of failures. Complicated analysis and deducing processes are also required. Reliability analysis and design for non-monotonic and dynamic control systems is difficult due to the complexity of the control algorithms. Simple methods are still needed due to the problems of uncertainty interference and failures. In addition, reliability analysis of control systems is still focused on FMECA or reliability tests for key objects or structures [19,32]. The reliability of dynamic control systems lacks quantitative evaluation methods.

The extended state observer (ESO) was first proposed by Han in [9] and has been the basis to form a new control technology that is known as active disturbance rejection control (ADRC). The total disturbance, including internal nonlinear dynamics, coupling effects, model inaccuracy, and external disturbance and uncertainties, is regarded as an extended state of the system to be observed. The estimated disturbance obtained by ESO will be used to compensate the control output to achieve disturbance rejection. Control of large uncertainties together with satisfactory performance can be achieved by ADRC due to the strong capability of ESO [29].

Since ESO was proposed, Gao [13] and some other scholars have made many efforts to improve ESO and ESO based control strategies. Fractional ADRC [13], linear ESO and linear ADRC [6], linear-nonlinear switching ADRC [15] and some other control methods based on ESO [16,20] were proposed. Yang et al. [31] used enhanced ESO and corresponding ADRC for a MIMO system, which could accelerate the response time. Xue et al. [29] proposed an adaptive ESO and applied it to air–fuel ratio control in gasoline engines. In [7] and [28], ESO was designed and utilized for fault diagnosis and fault-tolerant control. Thus far, applications of ESO based control strategies have proven its superiority in dealing with uncertainties and disturbances [1,14,18]. Moreover, the stability of ESO has also been analyzed and theoretically proven [11]. Performance [21,30] and limits [10,26] were also analyzed. Considering the merits of ESO, the distributed ESO based control strategy provides an effective solution to the uncertain disturbance and failure problems of the multi-legged mobile robot level adjustment control system.

In this paper, a multi-ESO based control strategy is proposed to promote the reliability of the quadruped robot level adjustment control system during disturbances and actuator failures. For parallel control objects, such as multiple legs, more ESOs were added to improve the disturbance rejection ability of the LADRC. Based on multiple linear ESOs, this novel method has superior parameter tuning and ability to deal with uncertainties. The information interaction between the actuators can be achieved by the integration of information from multiple ESOs. Motion reliability indicators have also been proposed to analyze and evaluate the reliability of motion control systems. A quantitative reliability evaluation method for the dynamic response of the control systems is designed and proposed. Simulation and experimental results show the satisfactory performance and reliability of the proposed method for addressing disturbances and failures.

The rest of this paper is organized as follows. Section 2 describes the design and process of the multi-ESO based control strategy in detail. Section 3 gives the control system reliability evaluation method. Section 4 introduces the plant, states the modeling process, and classifies typical failure conditions. Section 5 presents the simulation results and reliability analysis systematically. Conclusions about the presented technique are given in Section 6.

2. Multi-ESO Based Control Method

2.1. Linear Active Disturbance Rejection Control

Nonlinear functions were designed and used in the original ADRC controller proposed by Han [9]. Although the performance of the nonlinear ADRC controller is very good, the parameter adjustment is complicated, and it is difficult to achieve simple and rapid control in practical applications. Gao [13 15] found through a large number of studies that proper linear functions can also obtain excellent performance for ADRC controllers, and the calculation of parameter tuning is greatly reduced, which is more suitable for engineering applications. The basic idea of the ADRC linear simplification is to linearize the ESO and relate its parameters to the observer bandwidth to simplify the ESO design. A simple PD control is used to correlate the proportional coefficient and the derivative time constant with the controller bandwidth to simplify controller tuning. A standard single ESO LADRC control scheme is shown in Fig. 1.

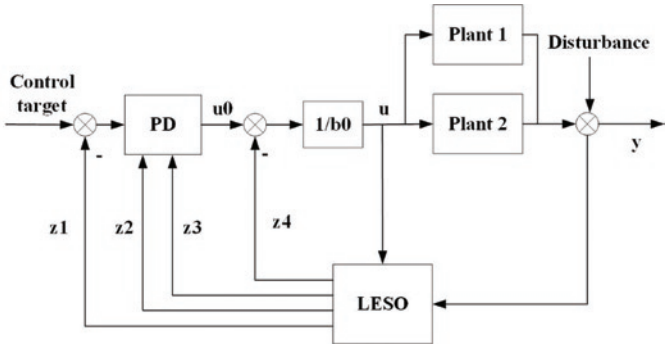

Fig. 1 Standard single ESO LADRC control scheme.

2.2. Design of the Extended State Observer

The linear extended state observer (LESO) is based on a simplified linear structure and uses the input and output of a system to estimate the extended system states. Because ADRC has the characteristics of being independent of the object model, the LESO can be designed as standard object model-free forms. In the case where a partial model of the object is known, a model-assisted LESO can be designed based on the known model information. Both the calculation of the ESO and the lag of the disturbance estimate can be reduced. Moreover, for an n-order system, the states estimated by the ESO contain the disturbance information, the system output and the 1 to n-1 order derivatives. When the system output and some low-order derivatives can be obtained, it is unnecessary to use the ESO to estimate these state variables; thus, the LESO structure can be simplified to obtain the reduced-order LESO. Standard object model-free LESO is adopted in this paper.

For an n-order system:

$$y^{(n)} = -a_{n-1}y^{(n-1)} - a_{n-2}y^{(n-2)} - \cdots - a_0 y + \omega + bu \qquad (1)$$

where u is the input, y is the output, and ω is the disturbance. a_0, $a_1, \ldots a_{n-1}$ are object structure parameters, which are unknown here. b is part known and the known part is denoted as b_0. Then, the above formula can be written as:

$$y^{(n)} = f + b_0 u \tag{2}$$

where f is the total disturbance of the system, including external and internal disturbances.

By expanding the total disturbance f to the n+1 state variable of the system, equation (2) can be transformed into an n+1 order extended state space description:

$$\begin{cases} \dot{x} = Ax + Bu + E\dot{f} \\ y = Cx \end{cases} \tag{3}$$

In which,

$$A = \begin{bmatrix} 0 & 1 & 0 & \cdots & 0 \\ 0 & 0 & 1 & \cdots & 0 \\ 0 & 0 & 0 & \cdots & 0 \\ \cdots & \cdots & \cdots & \cdots & 1 \\ 0 & 0 & 0 & \cdots & 0 \end{bmatrix}_{(n+1)\times(n+1)} \quad B = \begin{bmatrix} 0 \\ 0 \\ \cdots \\ b_0 \\ 0 \end{bmatrix}_{(n+1)\times 1} \quad E = \begin{bmatrix} 0 \\ 0 \\ \cdots \\ 0 \\ 1 \end{bmatrix}_{(n+1)\times 1}$$

$$C = \begin{bmatrix} 1 & 0 & 0 & \cdots & 0 \end{bmatrix}_{1\times(n+1)}$$

The corresponding LESO is:

$$\begin{cases} \dot{z} = Az + Bu + L(y - Cz) \\ \dot{y} = Cz \end{cases} \tag{4}$$

where $z \to x$ is the observer state vector and L is the observer error feedback gain matrix. Using $L = \begin{bmatrix} l_1 & l_2 & \cdots & l_{n+1} \end{bmatrix}^T$, the observer characteristic polynomial is:

$$s^{n+1} + l_1 s^n + \cdots + l_{n+1} = (s + \omega_0)^{n+1} \tag{5}$$

Discretization is needed for computer simulation. The object of this paper is a third-order system. The Euler method is used to discretize the LESO, and the fourth-order discrete LESO is constructed as:

$$\begin{cases} z(k+1) = \Phi_E z(k) + \Gamma_E u_d(k) \\ y_d(k) = \mathrm{H}_E z(k) + L_E u_d(k) \end{cases} \tag{6}$$

where:

$$\Phi_E = \begin{bmatrix} 1-(l_1+l_2h) & h & 0 & 0 \\ -(l_2+l_3h) & 1 & h & 0 \\ -(l_3+l_4h) & 0 & 1 & h \\ -l_4 & 0 & 0 & 1 \end{bmatrix} \quad \Gamma_E = \begin{bmatrix} 0 & l_1+l_2h \\ 0 & l_2+l_3h \\ b_0h & l_3+l_4h \\ 0 & l_4 \end{bmatrix}$$

$$\mathrm{H}_E = \begin{bmatrix} 1-l_1h & 0 & 0 & 0 \\ -l_2h & 1 & 0 & 0 \\ -l_3h & 0 & 1 & 0 \\ -l_4h & 0 & 0 & 1 \end{bmatrix} \quad L_E = \begin{bmatrix} 0 & l_1 \\ 0 & l_2 \\ 0 & l_3 \\ 0 & l_4 \end{bmatrix} \quad u_d(k) = \begin{bmatrix} u(k) \\ y(k) \end{bmatrix}$$

And h is the system sampling time.

Let $\beta = e^{-\omega_0 h}$, and then:

$$\begin{cases} l_1 = 1 - \beta^4 \\ l_2 = \dfrac{1}{h}(\beta^4 - 4\beta + 3) \\ l_3 = \dfrac{1}{h^2}(-\beta^4 + 6\beta^2 - 8\beta + 3) \\ l_4 = \dfrac{1}{h^3}(4\beta^4 - 4\beta^3 + 5\beta^2 - 4\beta + 1) \end{cases} \tag{7}$$

2.3. Design of the Multi-ESO Based Control Strategy

In this section, a multi-ESO based linear active disturbance rejection control strategy is proposed. The anti-interference ability of the LADRC is utilized, and the system can cope with the overall environmental disturbance. However, the control signals sent to a group of plants are fixed and cannot be adjusted according to the situation of each plant, so the performance under actuator failure may be unsatisfactory. The control strategy we proposed designs an ESO for each plant, and the PD part shares the same. Considering the same structure of plants in this paper, the parameters of each ESO can be the same as well, which will not increase the number of parameters of the entire LADRC control strategy. The control signals received by each plant can be dynamically adjusted based on different state observations and estimates, which may further improve the disturbance rejection and fault tolerance of the LADRC. The structure of the proposed multi-ESO based LADRC strategy is shown in Fig. 2.

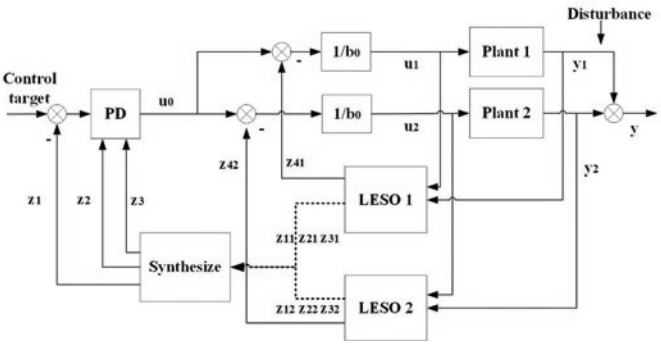

Fig. 2 The multi-ESO based LADRC strategy.

In the multi-ESO based control strategy, LESO 1 and LESO 2 use the design in Section 2.2. Here, the input and output of LESO 1 are u_1, y_1 and z_{11}, z_{21}, z_{31}, z_{41}, respectively. The input and output of LESO 2 are u_2, y_2 and z_{12}, z_{22}, z_{32}, z_{42}, respectively. As the estimated total disturbances of plant 1 and plant 2, z_{41} and z_{42} are used to compensate the control signals. z_1, z_2, and z_3 are the system states estimated by the observers after synthesis. Since $z_{11} \to y_1, z_{21} \to \dot{y}_1, z_{31} \to \ddot{y}_1, z_{12} \to y_2, z_{22} \to \dot{y}_2, z_{32} \to \ddot{y}_2$ and $z_1 \to y, z_2 \to \dot{y}, z_3 \to \ddot{y}$, the synthesized part should be designed according to the relationship among y_1, y_2, and y. In this paper, $y = y_1 + y_2$, therefore:

$$\begin{cases} y = y_1 + y_2 \\ \dot{y} = \dot{y}_1 + \dot{y}_2 \\ \ddot{y} = \ddot{y}_1 + \ddot{y}_2 \end{cases} \tag{8}$$

and

$$\begin{cases} z_1 = z_{11} + z_{12} \\ z_2 = z_{21} + z_{22} \\ z_3 = z_{31} + z_{32} \end{cases} \tag{9}$$

The PD part is designed as follows:

$$u_0 = k_p(r - z_1) - k_{d1}z_2 - k_{d2}z_3 \tag{10}$$

where r is the control target. The controller gain matrix is $\mathbf{K}=[k_{d2} \quad k_{d1} \quad k_p]^T$, and thus, the system characteristic polynomial is:

$$s^3 + k_{d2}s^2 + k_{d1}s + k_p = (s + \omega_c)^3 \tag{11}$$

After discretization, the output u_0 of the PD part is:

$$u_0 = \omega_c{}^3 z_1 - 3\omega_c{}^2 z_2 - 3\omega_c z_3 \tag{12}$$

Then, the control signal to the actuators is:

$$u_1 = \frac{u_0 - z_{41}}{b_0} \tag{13}$$

$$u_2 = \frac{u_0 - z_{42}}{b_0} \tag{14}$$

Thus, the multi-ESO based control strategy only needs to adjust the controller bandwidth ω_c, the observer bandwidth ω_0, and b_0 for a total of three parameters. The controller bandwidth ω_c determines the response speed of the controller. When the value is within an appropriate range, the larger the value of ω_c, the better the system control effect is. However, excessively large ω_c may cause the system to be unstable. The observer bandwidth ω_0 affects the tracking speed of the state observer. The tracking speed of the state observer increases with increasing ω_0, but an overly large speed could cause oscillation or noise. b_0 represents the characteristics of the object.

3. Control System Reliability Evaluation Method

To analyze and evaluate the reliability of the control systems after failure occurs, the following reliability evaluation indicators are given:

(1) Stability reliability, R_s

$$R_s = \frac{U_M}{U_R} \tag{15}$$

In which U_M is the stable controlled angular range under failures, U_R is the demanded stable controlled angular range.

The stability reliability reflects the controllability of the control system under fault conditions. Within the stable controlled angular range, the system is still stable and will not have a fatal stable fault.

(2) Steady state reliability, R_r

$$R_r = \begin{cases} \frac{1-e_f}{1-e_o} & (e_f > e_o) \\ 1 & (e_f \le e_o) \end{cases} \tag{16}$$

where e_o is the steady-state error of the control system without faults, and e_f is the steady-state error of the control system under fault conditions (with the maximum disturbance under control).

Steady-state reliability reflects the ability of the control system to maintain control accuracy under fault conditions.

(3) Transient reliability, R_t

$$R_t = \begin{cases} \frac{1-\sigma_f}{1-\sigma_o} & (\sigma_f > \sigma_o) \\ 1 & (\sigma_f \le \sigma_o) \end{cases} \tag{17}$$

In which σ_o is the overshoot of the control system without faults, and σ_f is the overshoot of the control system under fault conditions (with the maximum disturbance under control).

Transient reliability reflects the stability of the control system under fault conditions.

(4) Time coefficient, t_R

$$t_R = \begin{cases} \frac{t_{so}}{t_{sf}} & (t_{sf} > t_{so}) \\ 1 & (t_{sf} \le t_{so}) \end{cases} \tag{18}$$

where t_{so} is the response time of the control system without faults, t_{sf} is the response time of the control system under fault conditions (with the maximum disturbance under control).

The time coefficient reflects the ability of the control system to maintain the response speed under fault conditions.

Based on the analysis above, the concept of the motion reliability of the motion control system can be proposed to evaluate the reliability of the control system.

Definition: The motion reliability of a motion control system refers to the ability of a system to maintain its control performance under specified conditions when a fault occurs, recorded as R_m.

This is calculated by:

$$R_m = R_s * R_r * R_t * t_R \tag{19}$$

4. System Analysis and Plant Modeling

4.1. Level Adjustment Control System of a Quadruped Robot

Mobile robots require good obstacle crossing ability and reliability to adapt to different terrains. A quadruped robot design is adopted and analyzed in this paper. A quadruped robot is equipped with four legs that can be moved up and down at the four corners of a square platform. The two legs on the diagonal are a group that can change the level adjustment of the robot platform in the diagonal direction. The main parts of the quadruped robot level adjustment control system are shown in Fig.3. In the level adjustment control system, the pose signal of the robot is detected by an altitude angle sensor and sent to the computer. Then, the control signal is sent to the controller after calculation. The legs follow the control commands to make the corresponding movements under the motor drive. When a platform slant is detected, the legs deform and attempt to reduce the tilt angle. This design helps the robot reduce the possibility of rollover and enhances stability when encountering obstacles.

The robot platform performs 3-dimensional space motion on the ground, and its degree of freedom is 3. To describe the altitude change of the platform, a space coordinate system needs to be established.

We use the following assumptions:

(1) The robot platform is a rigid body;
(2) The geometric center and center of gravity of the platform are coincident;
(3) The change in the heading angle of the robot platform during movement is small and can be ignored.

Based on the above assumptions, the established spatial coordinate system describing the altitude of the platform includes two coor-

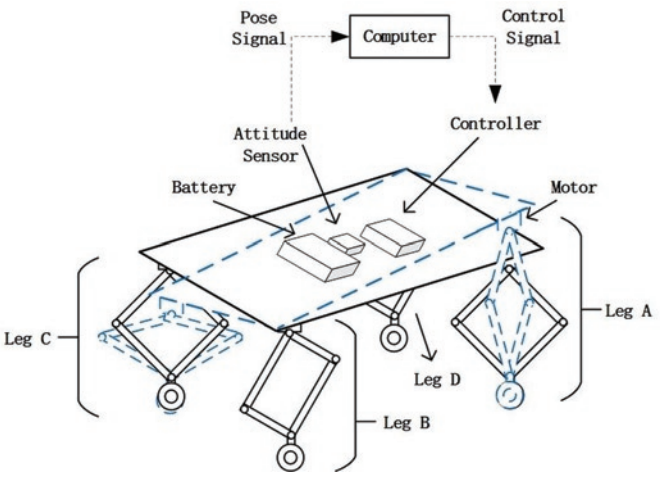

Fig. 3. Main parts of a quadruped robot level adjustment control system

dinate systems, the inertial coordinate system E-XYZ and the follower coordinate system B-XYZ, which are shown in Fig. 4. The origin of E-XYZ is the geometric center of the platform when the height of the platform is half of the maximum height from the ground. East of the origin is the X-axis positive direction (*Xe*), north is the Y-axis positive direction (*Ye*), and vertical to the ground is the Z-axis positive direction (*Ze*). For the B-XYZ coordinate system, the origin is at the geometric center of the platform. The direction of the platform geometric center pointing to leg A is the X-axis positive direction (*Xb*), the direction of the geometric center pointing to leg B is the Y-axis positive direction (*Yb*), and the direction perpendicular upward to the plane formed by *Xb* and *Yb* and through the geometric center is the Z-axis positive direction (*Zb*).

Define $q=(\Phi, \Theta, \Psi, x, y, z)^T$ as the generalized coordinate vector of the robot platform relative to the inertial coordinate system E-XYZ. $\eta=(\Phi, \Theta, \Psi)^T$ is the Euler angle that describes the attitude angle, in which Φ, Θ, Ψ represent the roll angle, pitch angle, and heading angle, respectively. $X=(x, y, z)^T$ stands for the spatial position vector of the platform centroid relative to the inertial coordinate system.

The length of legs A and C of the robot will control the roll angle of the platform. When the length of leg A is greater than that of leg C, the platform will have a positive roll angle ($\Phi>0$). In contrast, if the length of leg A is less than that of leg C, the platform will have a negative pitch angle ($\Phi<0$).

Similarly, the length of legs B and D on the robot will control the pitch angle of the platform. When the length of leg B is greater than that of leg D, the pitch angle is $\Theta>0$. When the length of leg B is less than that of leg D, the pitch angle is $\Phi<0$.

4.2. Plant Modeling

Each leg of the robot consists of two identical branches, each of which includes the upper part and the lower part. The structure of a leg is shown in Fig. 5. The length of the upper part is *L1,* and the lower part is *L2*. The two upper parts of each leg are driven by the motors and rotate around the *O* point for active motion. The two lower sections are hinged together for passive motion. Theoretically, the angle change of ϕ_1 and ϕ_2, which is the change in the rotation angle of the two upper parts, can realize the length change between *L2-L1* and *L2+L1* for each leg.

The whole structure of the leg turns the electric energy of a battery into the rotational angular velocity of the leg. According to the bond graph theory, the bond graph model for each leg can be obtained as shown in Fig. 6. Bond graph models can be transformed into a block diagram and simulated [33]. Using this method, a block diagram simulation model of the leg structure can be obtained without deriving its transfer function. The dynamic constraints of the object are embedded

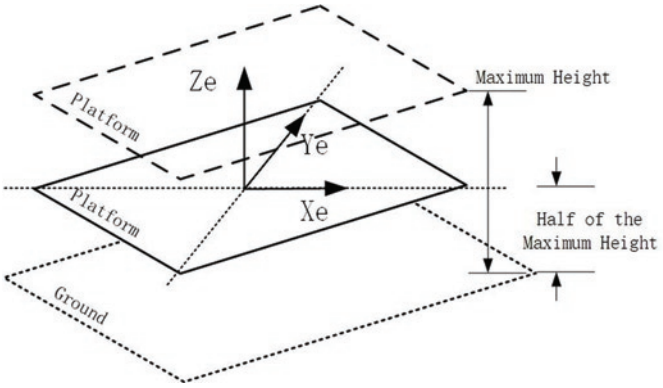

a) The E-XYZ coordinate system

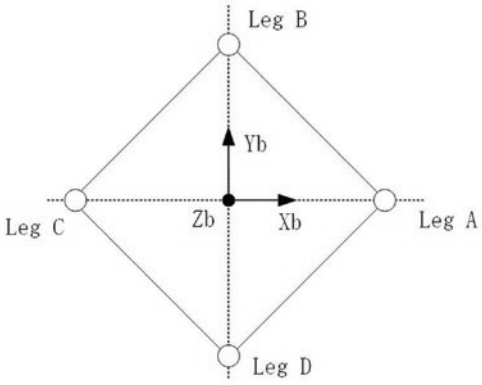

(b) The B-XYZ coordinate system

Fig. 4. Coordinate systems

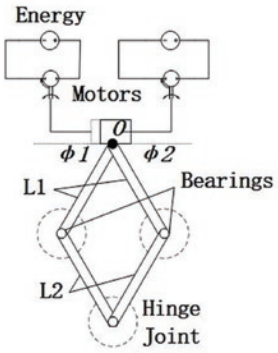

Fig. 5. The structure of a leg

Table1. List of Model Parameters

Description	Symbol	Value
Motor input voltage	Se	12 V
Motor output gear radius	r	0.025 m
Motor inductive reactance	R	1 Ω
Bearing and Hinge damping	b1 b2	4 N.s/m
Leg elastic coefficient	k	8 N/m
Length of the upper part	L1	0.1 m
Mass of the upper part	m1	0.1 kg
Length of the lower part	L2	0.1 m
Mass of the lower part	m2	0.1 kg
Bearing mass	m	0.01 kg

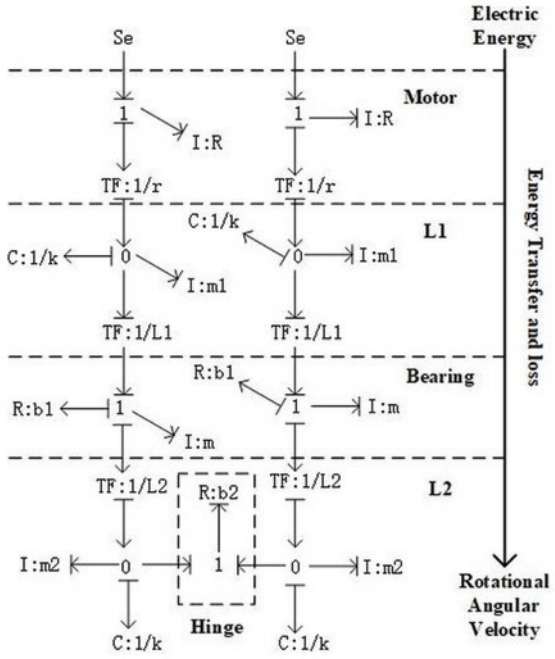

Fig. 6. Bond graph model of a leg

in the bond graph modeling rules. The parameters used in the simulation model are shown in TABLE 1.

4.3. Classification of Failure Conditions

Legs or motors being stuck is the most likely failure mode during operation of the level adjustment control process of a quadruped robot. Leg stuck failure will lead to a lower ability to resist disturbances or the inability to pass obstacles. We determined three kinds of leg stuck failure states in the control process of the quadruped robot, denoted by states A, B, and C.

Failure state A indicates that the failure occurs at the same time as the disturbance. The leg will be at the initial position and cannot follow the instructions of the controller.

Failure state B indicates that stuck failure occurs when the leg moves to the maximum length and stops during the control process.

Failure state C indicates that the failure occurs after one interference and when facing another. The leg will be stuck at the last position after one adjustment. Then, a disturbance is applied again to the control system. This failure state includes two cases, i.e., dealing with a small interference first and dealing with a large interference first.

The failure conditions during the level adjustment control process are shown in Fig.7. The latter simulation analysis will analyze the

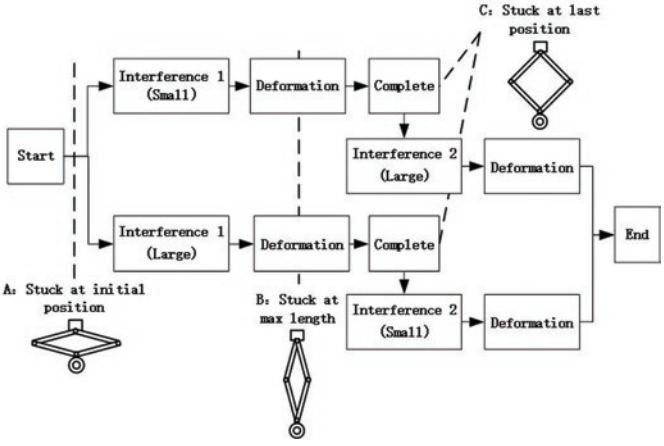

Fig.7 Failure conditions during the level adjustment control process

control performance and reliability of the proposed method from the perspective of these three types of faults.

5. Reliability Analysis

5.1. Simulation Results

With the system model and the multi-ESO based control strategy, the simulation was established in MATLAB/simulink. Considering the ability of the actual system and the actuators, the corresponding limiting module was added to the system simulation model. With the strong robustness and performance of the ESO based control method, the parameters were easily obtained through tuning in the simulation, and relatively good parameters were set as ω_c=21, ω_0=42, and b_0=380. The standard LADRC control scheme uses the same parameters as the multi-ESO-based control method.

Based on the information above, the simulation curves under normal conditions without leg failures are plotted in Fig. 8. The dashed lines in the figure are the responses of the standard LADRC control scheme, and the solid lines are the responses of the proposed multi-ESO based control strategy. The results illustrate that the two control strategies perform well without leg failures under disturbances of 10° and 20°. The response time is less than 2 seconds. Overall, the responses of the new method are slightly inferior to those of the standard LADRC due to the increased complexity of the structure in the multi-ESO based control method. For failure-free situations that do not require flexible changes of the control scheme, the simple method performs better. Under the 20° disturbance, the e_o of the LADRC and multi-ESO control is 0, the σ_o of LADRC is 12.5% and the σ_o of multi-ESO is 15%, and the t_{so} of LADRC and multi-ESO is 1.5 s. Next, the performance of the control strategies under leg stuck failure conditions will be analyzed and discussed.

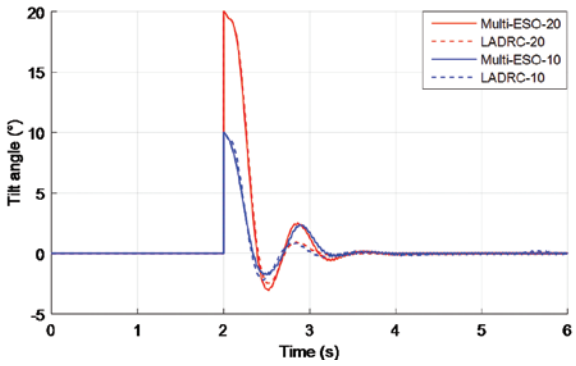

Fig. 8 Simulation results under normal conditions.

(1) Failure state A

In failure state A, the leg is stuck in the initial position and cannot follow the instructions of the controller, which may reduce the disturbance rejection ability of the level adjustment control system. The performances of the multi-ESO based control strategy and the standard LADRC scheme in failure state A are shown in Fig. 9. Both methods can handle 20 degree tilt angle interference under the conditions of failure state A. The response time of the systems when failure state A occur appears to be longer than that under normal conditions, which takes nearly 3 seconds. Under small angle interference (10°), the performances of the two control methods are basically the same. However, when the interference is large (20°), the response of the multi-ESO based control method is significantly better than that of the standard LADRC, with a smaller amplitude and faster response time. In view of the performances of the two methods, it is better to adopt the proposed multi-ESO based control strategy in failure state A. In this situation under 20° disturbance, the e_f of LADRC and multi-ESO

control is 0, the σ_f of LADRC is 32.5% and σ_f of multi-ESO is 12.5%, and the t_{sf} of LADRC is 2.5 s and that of multi-ESO is 1.8 s.

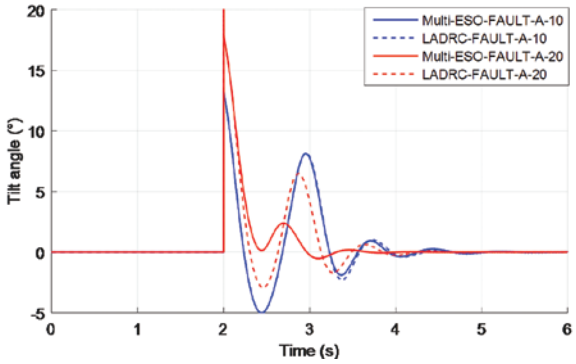

Fig. 9. Simulation results in failure state A

(2) Failure state B

In failure state B, the leg is stuck at the maximum length during the control process. This kind of large angle stuck failure may cause a significant drop in the system disturbance rejection ability. Fig. 10 shows the system responses of the multi-ESO based control strategy and the standard LADRC control scheme in failure state B. Both methods can handle 20 degree tilt angle interference under failure state B, and the response time is a little longer than that under normal conditions. The oscillation of the system response is much worse than that under normal conditions. The responses to the 20 degree interference are better than those to the 10 degree interference because the stuck position is close to the required position of the controller to the leg to resist the disturbance. However, the anti-interference ability of the system still decreases under failure state B. It can be seen clearly that the control quality of the proposed multi-ESO based control strategy is quite good and has advantages over the standard LADRC when failure state B occurs. In this situation, under a 20° disturbance, the e_f of LADRC and multi-ESO control is 0, the σ_f of LADRC is 60% and the σ_f of multi-ESO is 15%, and the t_{sf} of LADRC is 2.6 s and that of multi-ESO is 1.6 s.

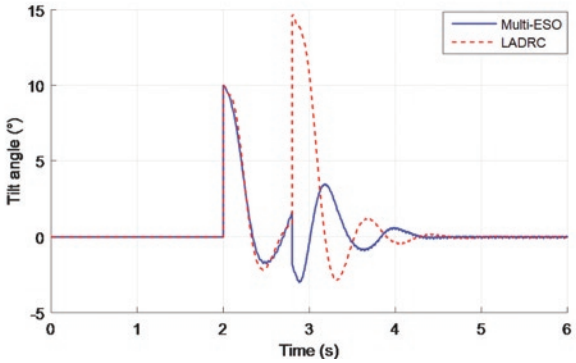

(a) Interference of 10 degrees

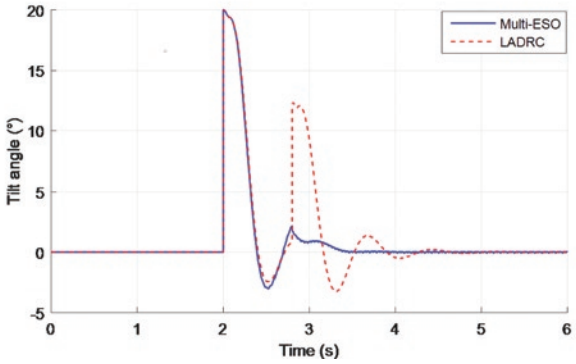

(b) Interference of 20 degrees

Fig. 10. Simulation results in failure state B

(3) Failure state C

In failure state C, the leg is stuck at the last position after one adjustment, and then, an interference is applied again to the control system. The simulation curves of the multi-ESO based control strategy and the standard LADRC scheme in failure state C are shown in Fig. 11. In Fig. 11(a), a small interference of 10 degrees was applied to the systems first, followed by a large interference of 20 degrees. In Fig. 11(b), the systems are dealing with the large interference first. Both methods are capable of handling 20 degree interference in both cases of failure state C. It is obvious that the control performance of the proposed multi-ESO based control is significantly stronger than that of the standard LADRC in the case of dealing with a small disturbance first and then a large disturbance. In this situation, the e_f of LADRC and multi-ESO control is 0, the σ_f of LADRC is 25% and σ_f of multi-ESO is 5%, and t_{sf} of LADRC is 2.5 s and that of multi-ESO is 1.8 s. In the case of a large interference first, the standard LADRC control is slightly better. Here, the e_f of LADRC and multi-ESO control is 0, the σ_f of LADRC is 50% and σ_f of multi-ESO is 55%, and t_{sf} of LADRC is 1.5 s and that of multi-ESO is 1.2 s. The reverse oscillation after stuck failure was injected may be due to the unexpected coupling calculation of the multi-ESO based control. Nevertheless, the degradation of the control quality of the multi-ESO based control strategy during stuck failure C is acceptable.

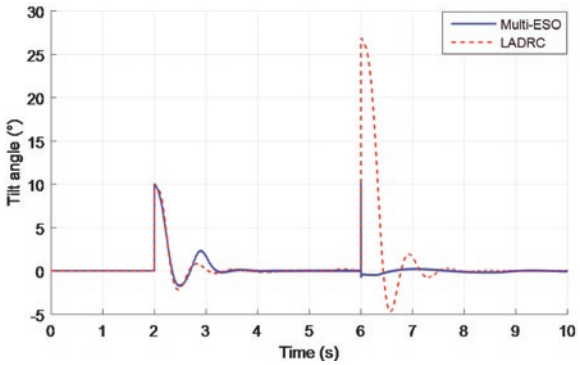

(a) First 10 degrees and then 20 degrees

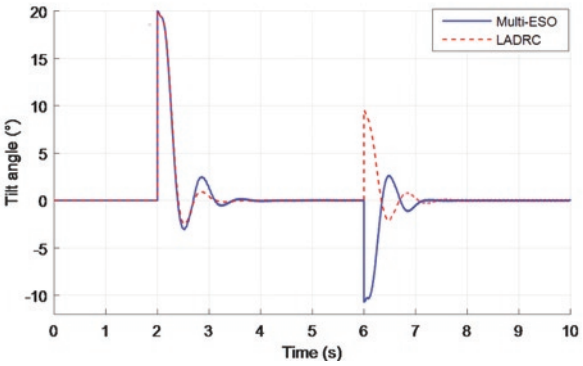

(b) First 20 degrees and then 10 degrees.

Fig. 11. Simulation results in failure state C

(4) Reliability Analysis

Based on the responses of the LADRC and multi-ESO control, the motion reliability of both methods can be calculated by equations (15)-(19), and the calculation results are shown in TABLE 2.

In the table, as in all the situations, the system could handle a disturbance of 20 degrees, and the steady-state errors are zero. The sta-

Table 2. Reliability Calculation of LADRC and Multi-ESO

Situation	Method	Overshoot, σ (%)	Response Time, ts (s)	Transient Reliability, R_t	Time Coefficient, t_R
Normal (20°)	LADRC	12.5	1.5	/	/
	m-ESO	15	1.5	/	/
Failure state A (20°)	LADRC	32.5	2.5	0.77	0.6
	m-ESO	12.5	1.8	1	0.83
Failure state B (20°)	LADRC	60	2.6	0.46	0.58
	m-ESO	15	1.6	1	0.94
Failure state C (10° first)	LADRC	25	2.5	0.86	0.6
	m-ESO	5	1.8	1	0.83
Failure state C (20° first)	LADRC	50	1.5	0.57	1
	m-ESO	55	1.2	0.53	1
Method	**Stability Reliability R_s**	**Steady State Reliability R_r**	**Transient Reliability R_t**	**Time Coefficient t_R**	**Motion Reliability R_m**
LADRC	1	1	0.46	0.58	0.2668
m-ESO	1	1	0.53	0.83	0.4399

bility reliability, R_s, and the steady state reliability, R_r, are 1 for both control methods. The transient reliability, R_t, and time coefficient, t_R, of both control methods take the minimum values under these fault conditions. From the calculation results in TABLE 2, it is obvious that the reliability of the proposed multi-ESO control is better than that of the LADRC under the fault conditions.

According to the system simulation results under normal conditions and several failure conditions, the flexible control output of the multi-ESO based control strategy gives it excellent performance when the standard LADRC performance is poor. Although in the cases of normal conditions or some simple failures, the control performance of the multi-ESO based control method is slightly worse than that of the standard LADRC. The proposed multi-ESO based control strategy will enable the quadruped robot level adjustment control system to better cope with the leg stuck failures and maintain its anti-interference ability.

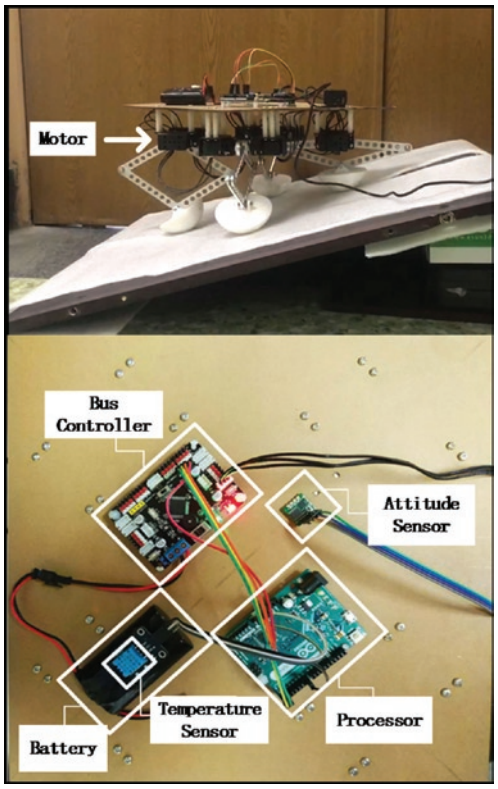

Fig. 12. Experimental setup

5.2. Pro-type Design and Experimental Validation

To show the effectiveness of the proposed multi-ESO based LADRC control solution in real time with leg failures, an experimental validation with the same structure introduced in Section 4 was set up in the laboratory as shown in Fig. 12. The tilt angle of the robot platform is detected by a JY-61 attitude sensor. The processor adopted was an Arduino Leonardo circuit board with an Atmega32u4 microcontroller. Eight ZX3615 motors were driven by a bus controller

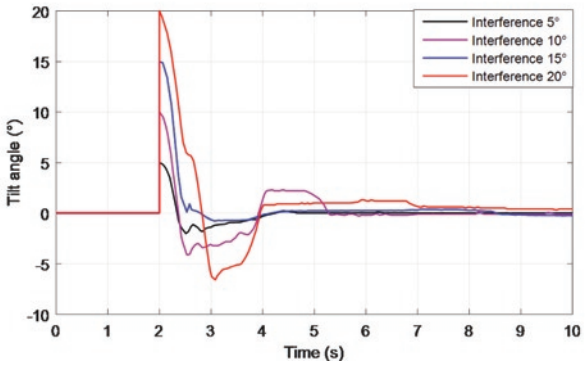

Fig. 13. Experimental results of the multi-ESO based control strategy under normal conditions

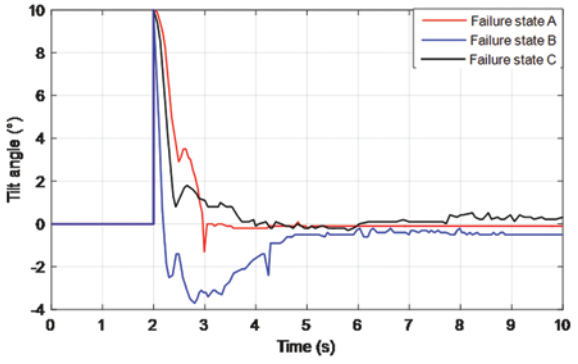

Fig. 14. Experimental results of the multi-ESO based control strategy under failure conditions

powered by batteries. The output voltage of the batteries is 12 V. To monitor the battery status, a temperature sensor was also added.

A robot using the multi-ESO based control algorithm was placed on slopes with inclinations of 5, 10, 15, and 20 degrees. The experimental curves of the robot platform tilt angles without leg failures were obtained by the computer program and are shown in Fig. 13. It can be seen that the system using the multi-ESO based control strategy can effectively overcome an external disturbance of no more than 20 degrees. The system altitude can quickly return to the target value with little overshoot, and the response time is short. Under large angle interference, the system response time is slightly longer, and there is a small static error, which is mainly due to hardware limitations. The results of the physical experiment are basically consistent with the simulation results.

The quadruped robot was placed on a 10 degree slope, and the leg stuck failures were injected by modifying the servo control command to obtain the system tilt angle output curves under failure conditions. Experimental results of the proposed multi-ESO based control strategy in failure states A, B and C are shown in Fig. 14. For failure state C, only the response to the second interference is shown. In the cases of failure state B and failure state C, there are slight jitters and static error in the system. According to the results, the robot could handle the disturbance with a leg stuck at different positions, which validates the effectiveness of the proposed control strategy.

6. Conclusion

In this paper, a multi-ESO based LADRC control strategy for the level adjustment control system of a quadruped robot is proposed and analyzed. By treating multiple legs as parallel control objects, the parameters of the ESO designed for each leg can be the same, which will not increase the number of parameters used in the LADRC control method. The control signals received by each leg can be dynamically adjusted due to the different state observations and estimates of each leg. For the reliability analysis, we took the condition of leg fault occurring into account and proposed a multidimensional reliability evaluation method for control systems. Control performance and reliability of the proposed multi-ESO based control strategy and the standard LADRC method were systematically simulated and compared. An experimental quadruped robot platform was established in the laboratory to show the effectiveness of the proposed multi-ESO based control solution in actual situations. The results illustrate that the proposed multi-ESO-based control method has the advantages of easy parameter tuning, good robustness, and strong ability to cope with disturbance and failure conditions. The proposed multi-ESO control method has more flexible control output to actuators, which can improve the reliability of the control system.

The main contributions of this paper are as follows:

(1) A multi-ESO based LADRC strategy for a level adjustment control system of a quadruped robot is proposed that could improve the fault tolerance of the LADRC under faults.

(2) A multi-dimensional reliability evaluation method for control systems was provided and used to analyze and evaluate the reliability of the proposed multi-ESO method under fault conditions. The steady state, transient and time characteristics of the control system can be comprehensively considered by this method, and the reliability of the control system response can be evaluated.

For future work, we would try to apply the multi-ESO control method to more objects. The synthesized part can be replaced by fuzzy modules or other intelligent methods.

References

1. Castaneda L, Luviano-Juarez A, Chairez I. Robust Trajectory Tracking of a Delta Robot Through Adaptive Active Disturbance Rejection Control. IEEE Transactions on Control Systems Technology 2015; 23(4): 1387-1398, https://doi.org/10.1109/TCST.2014.2367313.
2. Christensen D, Schultz U, Stoy K. A distributed and morphology-independent strategy for adaptive locomotion in self-reconfigurable modular robots. Robotics & Autonomous Systems 2013; 61(9): 1021-1035, https://doi.org/10.1016/j.robot.2013.05.009.
3. Cong Z. Distributed ESO based cooperative tracking control for high-order nonlinear multi-agent systems with lumped disturbance and application in multi flight simulators systems. Isa Transactions 2018; 74: 217-228, https://doi.org/10.1016/j.isatra.2018.01.020.
4. Cui J, Zeng S, Ren Y, Chen X, Gao Z. On the robustness and reliability in the pose deformation system of mobile robots. IEEE Access 2018, https://doi.org/10.1109/ACCESS.2018.2835836.
5. Cully A, Clune J, Tarapore D, Mouret J. Robots that can adapt like animals. Nature 2015; 521(7553): 503-507, https://doi.org/10.1038/nature14422.
6. Du B, Wu S, Han S, Cui S. Application of Linear Active Disturbance Rejection Controller for Sensorless Control of Internal Permanent-Magnet Synchronous Motor. IEEE Transactions on Industrial Electronics 2016; 63(5): 3019-3027, https://doi.org/10.1109/TIE.2016.2518123.
7. Falconi G, Heise C, Holzapfel F. Fault-tolerant position tracking of a hexacopter using an Extended State Observer. International Conference on Automation, Robotics and Applications. IEEE 2015; 550-556, https://doi.org/10.1109/ICARA.2015.7081207.
8. Gonzalez-Prieto I, Duran M, Barrero F. Fault-Tolerant Control of Six-Phase Induction Motor Drives With Variable Current Injection. IEEE Transactions on Power Electronics 2017; 32(10): 7894-7903, https://doi.org/10.1109/TPEL.2016.2639070.
9. Han J. From PID to active disturbance rejection control. IEEE Transactions on Industrial Electronics 2009; 56(3): 900-906, https://doi.org/10.1109/TIE.2008.2011621.
10. Herbst G. Practical Active Disturbance Rejection Control: Bumpless Transfer, Rate Limitation, and Incremental Algorithm. IEEE Transactions on Industrial Electronics 2016; 63(3): 1754-1762, https://doi.org/10.1109/TIE.2015.2499168.
11. Huang Y, Xue W. Active disturbance rejection control: Methodology and theoretical analysis. ISA Transactions 2014; 53(4): 963-976, https://doi.org/10.1016/j.isatra.2014.03.003.
12. Kommuri S, Defoort M, Karimi H, Veluvolu K. A Robust Observer-Based Sensor Fault-Tolerant Control for PMSM in Electric Vehicles. IEEE Transactions on Industrial Electronics 2016; 63(12): 7671-7681, https://doi.org/10.1109/TIE.2016.2590993.
13. Li D, Ding P, Gao Z. Fractional active disturbance rejection control. ISA Transactions 2016; 62: 109-119, https://doi.org/10.1016/j.isatra.2016.01.022.
14. Li D, Li C, Gao Z, Jin Q. On active disturbance rejection in temperature regulation of the proton exchange membrane fuel cells. Journal of Power Sources 2015; 283: 452-463, https://doi.org/10.1016/j.jpowsour.2015.02.106.
15. Li J, Xia Y, Qi X, Gao Z. On the Necessity, Scheme and Basis of the Linear-Nonlinear Switching in Active Disturbance Rejection Control. IEEE Transactions on Industrial Electronics 2017; 64(2): 1425-1435, https://doi.org/10.1109/TIE.2016.2611573.
16. Liu F, Li Y, Cao Y, She J, Wu M. A Two-Layer Active Disturbance Rejection Controller Design for Load Frequency Control of Interconnected

Power System. IEEE Transactions on Power Systems 2016; 31(4): 3320-3321, https://doi.org/10.1109/TPWRS.2015.2480005.
17. Ma X, Sun F, Li H, He B. Neural-network-based integral sliding-mode tracking control of second-order multi-agent systems with unmatched disturbances and completely unknown dynamics. International Journal of Control, Automation and Systems 2017; 15(4): 1925-1935, https://doi.org/10.1007/s12555-016-0057-z.
18. Madonski R, Kordasz M, Sauer P. Application of a disturbance-rejection controller for robotic-enhanced limb rehabilitation trainings. ISA Transactions 2014; 53(4): 899-908, https://doi.org/10.1016/j.isatra.2013.09.022.
19. Marina S, Franc N, Gregor P. Sensors in proactive maintenance - a case of LTCC pressure sensors. Eksploatacja i Niezawodnosc - Maintenance and Reliability 2018; 20(2): 267-272, https://doi.org/10.17531/ein.2018.2.12.
20. Ramos G, Cortes-Romero J, Coral-Enriquez H. Spatial observer-based repetitive controller: An active disturbance rejection approach. Control Engineering Practice 2015; 42: 1-11, https://doi.org/10.1016/j.conengprac.2015.05.002.
21. Ran M, Wang Q, Dong C. Stabilization of a class of nonlinear systems with actuator saturation via active disturbance rejection control. Automatica 2016; 63: 302-310, https://doi.org/10.1016/j.automatica.2015.10.010.
22. Rymarczyk T, Klosowski G. Innovative methods of neural reconstruction for tomographic images in maintenance of tank industrial reactors. Eksploatacja i Niezawodnosc - Maintenance and Reliability 2019; 21(2): 261-267, https://doi.org/10.17531/ein.2019.2.10.
23. Song Y, Guo J. Neuro-Adaptive Fault-Tolerant Tracking Control of Lagrange Systems Pursuing Targets With Unknown Trajectory. IEEE Transactions on Industrial Electronics 2017; 64(5): 3913-3920, https://doi.org/10.1109/TIE.2016.2644606.
24. Su X, Liu X, Song Y. Fault-Tolerant Control of Multi-area Power Systems via a Sliding-Mode Observer Technique. IEEE/ASME Transactions on Mechatronics 2018; 23(1): 38-47, https://doi.org/10.1109/TMECH.2017.2718109.
25. Shen Q, Wang D, Zhu S, Poh E. Robust Control Allocation for Spacecraft Attitude Tracking Under Actuator Faults. IEEE Transactions on Control Systems Technology 2017; 25(3): 1068-1075, https://doi.org/10.1109/TCST.2016.2574763.
26. Wu D, Chen K. Limit cycle analysis of active disturbance rejection control system with two nonlinearities. ISA Transactions 2014; 53(4): 947-954, https://doi.org/10.1016/j.isatra.2014.03.001.
27. Xiao B, Yin S. Velocity-Free Fault-Tolerant and Uncertainty Attenuation Control for a Class of Nonlinear Systems. IEEE Transactions on Industrial Electronics 2016; 63(7): 4400-4411, https://doi.org/10.1109/TIE.2016.2532284.
28. Xu C, Li J, Zhang P, Mu L, Si X. ESO-based fault diagnosis and fault-tolerant for incipient actuator faults. Control and Decision Conference. IEEE 2013; 4359-4363.
29. Xue W, Bai W, Yang S, Song K, Huang Y, Xie H. ADRC With Adaptive Extended State Observer and its Application to Air-Fuel Ratio Control in Gasoline Engines. IEEE Transactions on Industrial Electronics 2015; 62(9): 5847-5857, https://doi.org/10.1109/TIE.2015.2435004.
30. Xue W, Huang Y. On performance analysis of ADRC for a class of MIMO lower-triangular nonlinear uncertain systems. ISA Transactions 2014; 53(4): 955-962, https://doi.org/10.1016/j.isatra.2014.02.002.
31. Yang X, Cui J, Lao D, Li D, Chen J. Input Shaping enhanced Active Disturbance Rejection Control for a twin rotor multi-input multi-output system (TRMS). ISA Transactions 2016; 62: 287-298, https://doi.org/10.1016/j.isatra.2016.02.001.
32. Yang Y, Huang H, Liu Y, Zhu S, Peng W. Reliability analysis of electrohydraulic servo valve suffering common cause failures. Eksploatacja i Niezawodnosc - Maintenance and Reliability 2014; 16(3): 354-359.
33. Yu B, Paassen A. Simulink and bond graph modeling of an air-conditioned room. Simulation Modelling Practice & Theory 2004; 12(1): 61-76, https://doi.org/10.1016/j.simpat.2003.12.001.
34. Zhou Y, Huang Z, Liu W, Li H, Liao H. A distributed ESO based cooperative current-sharing strategy for parallel charging systems under disturbances. IEEE Energy Conversion Congress & Exposition 2016, https://doi.org/10.1109/ECCE.2016.7854675.

Jingjing CUI
Yi REN
Binghui XU
Dezhen YANG
Shengkui ZENG
School of Reliability and Systems Engineering
Beihang University
No.37 Xueyuan RD. Haidian, 100191, Beijing, China

E-mails: cuijingjing@buaa.edu.cn, renyi@buaa.edu.cn, xubinghui@buaa.edu.cn, dezhenyang@buaa.edu.cn, zengshengkui@buaa.edu.cn